Supplementary Information

Halide Ion Influence on the Formation of Nickel Nanoparticles and their Conversion into Hollow Nickel Phosphide and Sulphide Nanocrystals

Rasmus Himstedt,[a] Dominik Hinrichs,[a] Joachim Sann,[bc] Anica Weller,[d] Georg Steinhauser [d] and Dirk Dorfs *[ae]

[a] *Institute of Physical Chemistry and Electrochemistry, Leibniz Universität Hannover, Callinstraße 3A, 30167 Hannover, Germany.*

[b] *Center for Materials Research (LaMa), Justus Liebig University Giessen, Heinrich-Buff-Ring 16, 35392 Gießen, Germany.*

[c] *Institute of Physical Chemistry, Justus Liebig University Giessen, Heinrich-Buff-Ring 17, 35392 Gießen, Germany.*

[d] *Institute of Radioecology and Radiation Protection, Leibniz Universität Hannover, Herrenhäuser Straße 2, 30419 Hannover, Germany.*

[e] *Cluster of Excellence PhoenixD (Photonics, Optics, and Engineering Innovation Across Disciplines), Hannover, Germany.*

1. TEM Overview Images of Ni Nanoparticles

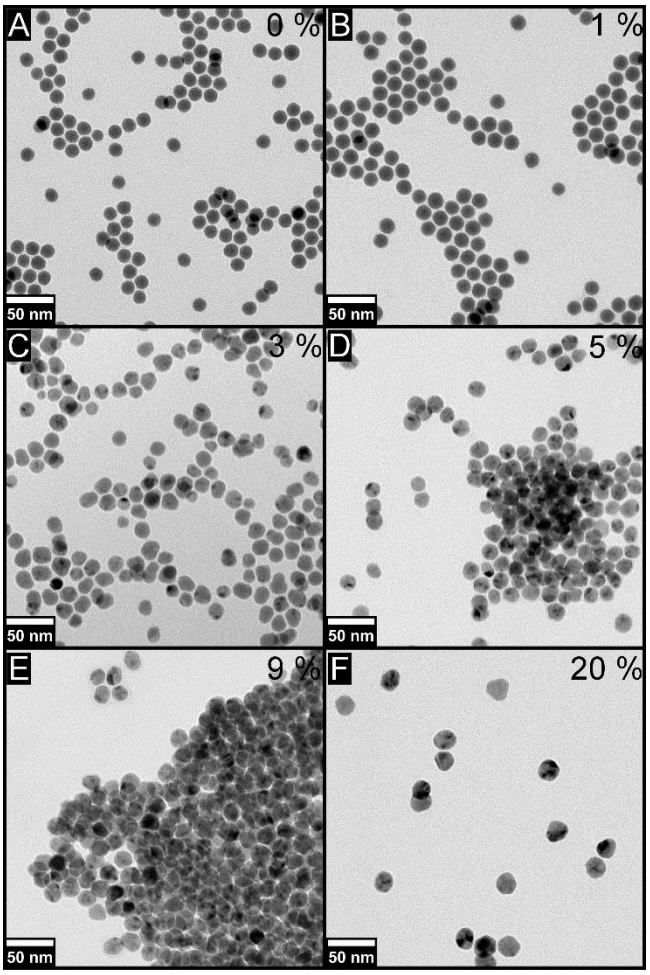

Fig. S1 TEM overview images of Ni nanoparticles synthesised in the presence of different concentrations of chloride ions. The influence of the chloride ions on the average particle diameter is negligible in the investigated concentration range. Only for high concentrations, a small increase is visible.

2. Investigation of the Phosphorus Content of Nanoparticles Synthesised in the Presence of Different Amounts of Cl^-

Selected area electron diffraction (SAED) measurements were conducted in case of the amorphous nanoparticles and revealed only fcc-Ni reflections (see Fig. S2A). This means small Ni crystallites are present in the particles. However, the content of the largely amorphous areas cannot be determined by this method. In order to investigate this, inductively coupled plasma mass spectrometry (ICP-MS) and X-ray photoelectron spectroscopy (XPS) measurements were performed in case of samples synthesised in the presence of different amounts of chloride. The XPS results show that phosphorus is present in form of nickel phosphates which most likely are located in the ligand shell of the nanoparticles or inside the organic layer surrounding them and also as nickel phosphide which could also have formed in the bulk of the particles. The ratio of phosphide to phosphate is decreasing with an increasing amount of used chloride (see Fig. 2B-G). The ICP-MS analysis, on the other hand, shows a large amount of phosphorus in the sample containing amorphous particles which is strongly decreased when chloride is used. Additionally, an attempt was made to measure the residual amount of chlorine in the samples but in case of all measured particle concentrations, the chlorine mass concentration was below the

detection limit of the device. Overall, these results, which are summarised in Tab. S1, show that while the amorphous nanoparticles contain a large amount of nickel phosphide (15 %), the presence of chloride during the particle synthesis stops the incorporation of P resulting in crystalline Ni nanoparticles. Also, the removal of chloride via the washing steps seems to be quantitative. Additionally, Fig. S3 shows the behaviour of the respective particle dispersions when confronted with a strong permanent magnet. While the meniscus of the solution containing the amorphous nanoparticles does not visibly change, the ones of the other solutions do react to the magnetic field. This is also indicative of the formation of nickel phosphide in the absence of chloride since the phosphorus incorporation likely severely alters the magnetic properties of the particles.

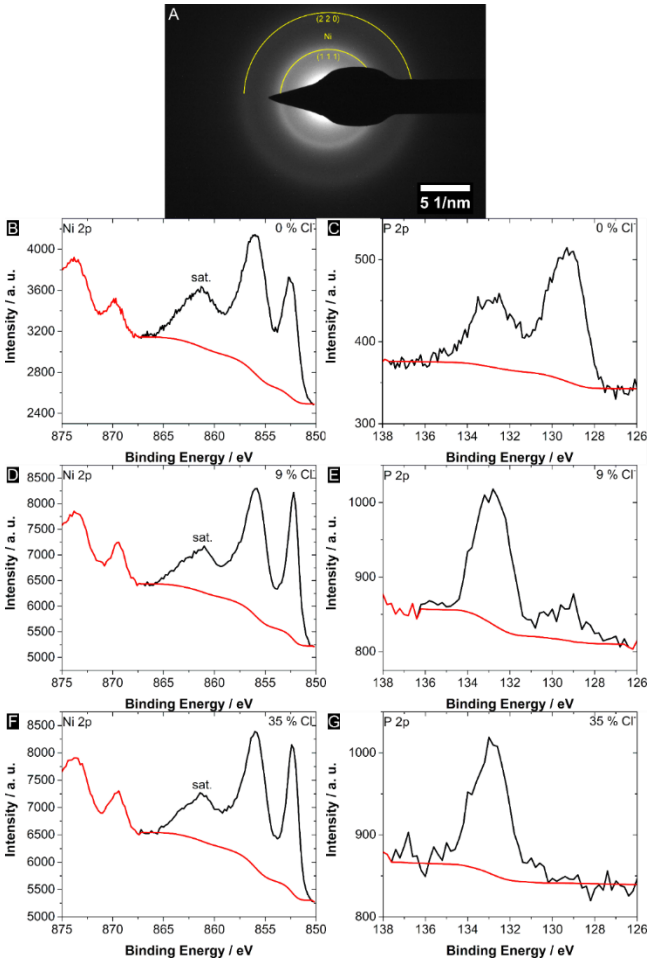

Fig. S2 (A) SAED image of a sample of X-ray-amorphous nanoparticles synthesised without any addition of halide ions to the reaction mixture. Very broad reflections, which correspond to the Ni (1 1 1) and (2 2 0) lattice planes, are visible. This result leads to the conclusion that very small Ni crystallites exist within the particles. (B), (D), (F) Ni 2p XPS spectra (black) of samples synthesised in the presence of 0, 9 and 35 % Cl^-, respectively. The background is shown as a red line. In addition to a satellite peak at 862 eV, two relevant peaks are visible. According to previous studies on TOP-capped Ni nanoparticles, which present very similar Ni 2p spectra, the peak at 856 eV corresponds to $Ni(OH)_2$ which forms on the particle surface.[1,2] However, the existence of nickel phosphate could also be responsible in this case.[3] The peak at 853 eV, on the other hand, is probably due to elemental Ni. It can be seen that compared to the X-ray amorphous particles the relative intensity of the latter peak is increased in case of the samples where chloride was used. (C), (E), (G) P 2p XPS spectra of the same samples. Again, two peaks are visible in case of the amorphous particles. The one at 133 eV corresponds to P in a high oxidation state like it is the case in phosphates while the peak at 129 eV is caused by nickel phosphides. It is obvious that while the majority of the phosphorus in the amorphous nanoparticles consists of phosphide (58.5 %), the addition of chloride to the nanoparticle synthesis leads to a continuous decrease of the phosphide fraction (22.6 % and 7.1 % for the samples with 9 and 35 % Cl^-, respectively).

Tab. S1 Total P and Ni contents of samples synthesised in the presence of different amounts of Cl^- determined by ICP-MS experiments as well as phosphide percentage of the P fraction measured via XPS. Using these results, the atomic percentage of phosphorus (as phosphide) inside the nickel nanoparticles could be calculated.

Used Cl^- amount / %	Ni/P Atom Ratio by ICP-MS	Fraction of Phosphide / %	P in Ni Particles / %
0	3.28	58.5	15.1
9	21.27	22.6	0.7
35	34.50	7.1	0.3

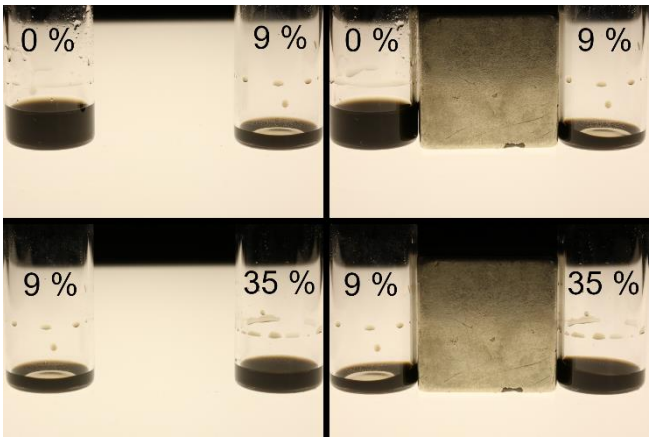

Fig. S3 Photographs of nanoparticle dispersions produced using different amounts of chloride during the synthesis without (left side) and in (right side) the presence of a neodymium magnet. It can be seen that the meniscus of the dispersion containing the amorphous particles does not visibly change while the others strongly react to the magnetic field.

3. TEM and XRD Analysis of Samples Synthesised with Different Cl^- Precursors

Different chloride ion precursors were used instead of TDAC. Like TDAC, chlorotriphenylmethane (CTPM) is decomposing under the reaction conditions and chloride ions are released. If it is added to the synthesis mixture the resulting nanoparticles look very similar. The crystallites grow larger the more chloride is present as shown by TEM and XRD analysis (see Fig. S4). In order to directly introduce solved chloride ions into the synthesis from the very beginning, the usual Ni precursor was also partly substituted by $NiCl_2{\cdot}6H_2O$. In this case, the trend is also the same and crystalline particles are obtained (see Fig. S5). Thus, except for little differences in the particle diameters, which could be due to a different solubility and therefore reactivity of the chloride sources in the used solvent, the nature of the precursor does not seem to have an important influence on the behaviour of the Ni nanoparticle system.

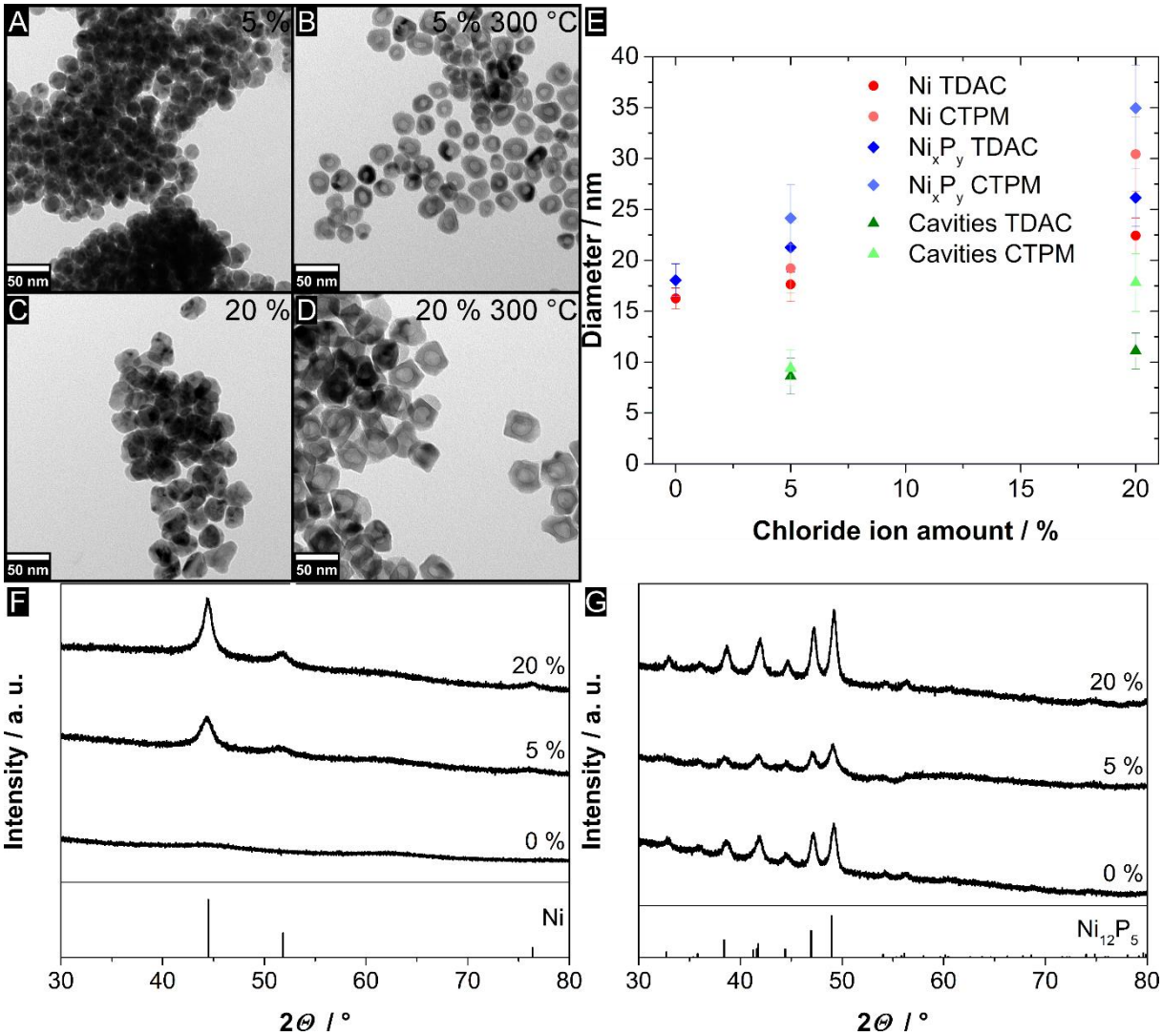

Fig. S4 TEM images of nanoparticles before and after crystallisation using different amounts of chlorotriphenylmethane (CTPM) as chloride ion precursor (A-D). The size of the particles and their shape anisotropy increases in case of the larger chloride ion concentration resulting in slightly different hollow nanoparticles after a subsequent crystallisation step at 300 °C when compared to the particles crystallised in the presence of tetradodecylammonium chloride (TDAC). (E) Dependence of the diameter of the shown nickel and nickel phosphide nanoparticles and their inner cavity on the type of chloride precursor present during their synthesis. The error bars correspond to the standard deviations of the measured diameters. It can be seen that the overall particle size is slightly increased with larger amounts of the halide. If CTPM is present the particles seem to grow larger than when the standard precursor TDAC is used, especially in case of larger amounts. (F) X-ray diffraction patterns of Ni nanoparticles synthesised with different amounts of CTPM as chloride ion precursor present. With an increasing chloride concentration, the Ni reflections (PDF card #: 01-087-0712) become more pronounced. (G) X-ray diffraction patterns of the corresponding nickel phosphide nanocrystals. In case of all the investigated chloride ion concentrations, the obtained nickel phosphide phase is $Ni_{12}P_5$ (PDF card #: 01-074-6017).

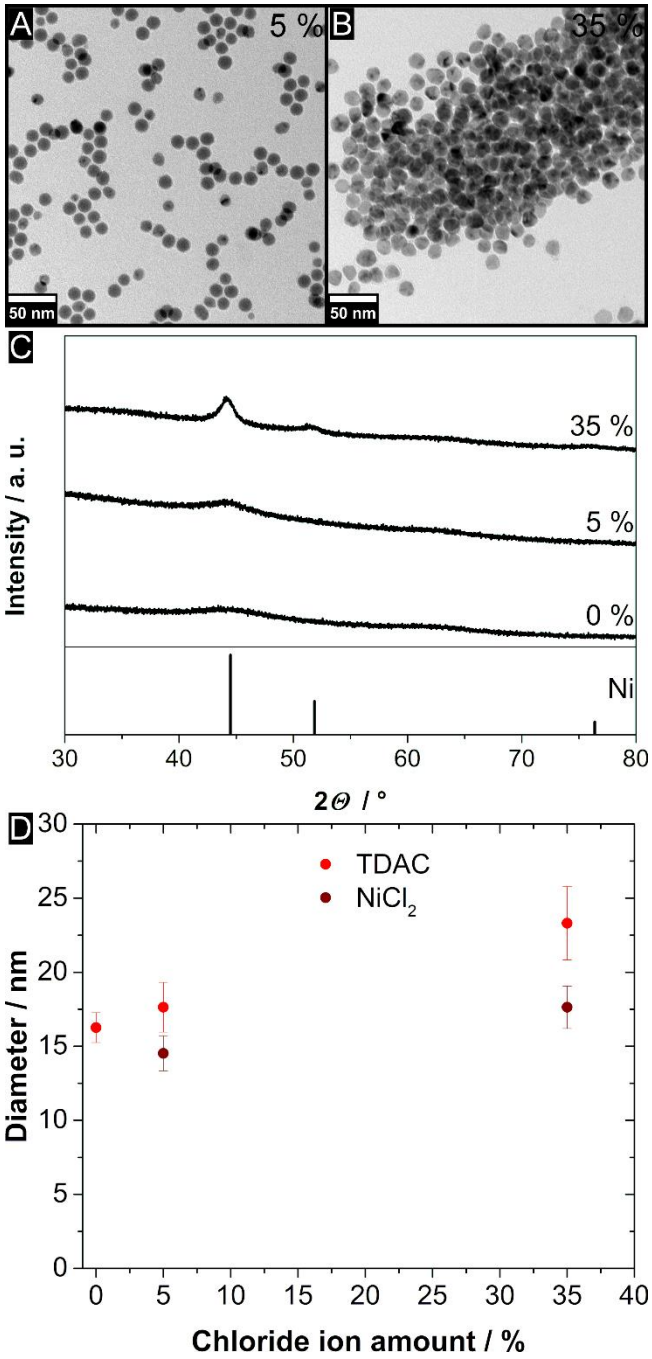

Fig. S5 TEM images of Ni nanoparticles synthesised by replacing different percentages of $Ni(acac)_2$ by $NiCl_2{\cdot}6H_2O$. With 2.5 % nickel chloride (5 % Cl^-) partially crystalline spherical Ni nanoparticles are obtained (A), while by using 17.5 % nickel chloride (35 % Cl^-) as Ni precursor fully crystalline particles are formed (B). (C) X-ray diffraction patterns of the respective particles. With an increasing chloride concentration, the Ni reflections (PDF card #: 01-087-0712) become more pronounced. They are, however, noticeably broader than the reflections of nanoparticles synthesised using different chloride sources, which could be explained by the smaller overall size of the nanocrystals. (D) Dependence of the diameter of the shown nickel nanoparticles on the type of chloride precursor present during their synthesis. The error bars correspond to the standard deviations of the measured diameters. It can be seen that the overall particle size is slightly increased with larger amounts of the halide. If $NiCl_2{\cdot}6H_2O$ is present the particles seem to turn out smaller than when the standard precursor tetradodecylammonium chloride (TDAC) is used, especially in case of larger amounts.

4. TEM and XRD Analysis of Samples Synthesised in the Presence of Br^-

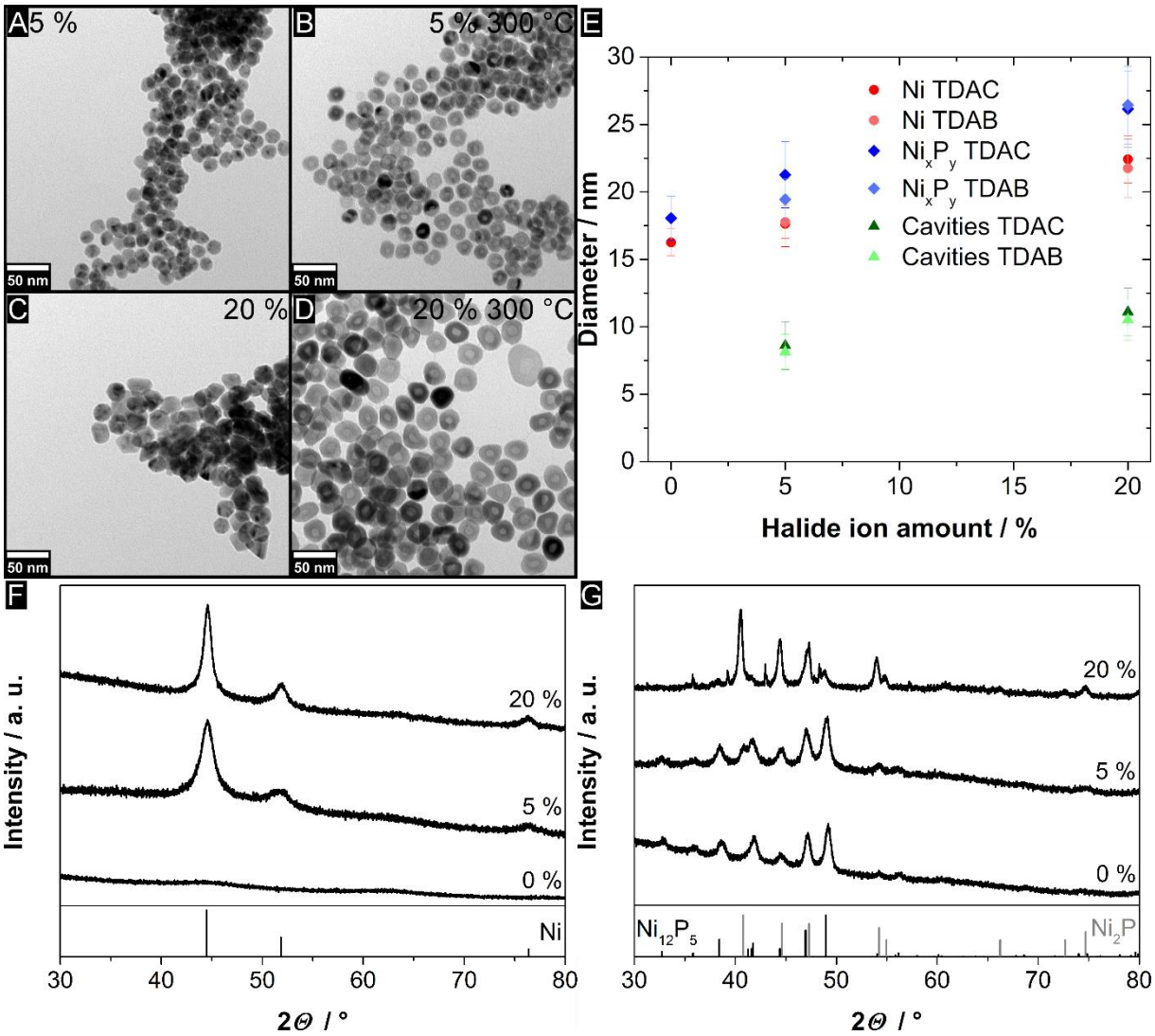

Fig. S6 TEM brightfield images of nickel nanoparticles synthesised in the presence of 5 % (A) and 20 % (C) bromine relative to nickel and of the resulting nickel phosphide nanocrystals after crystallisation at 300 °C (B and D, respectively). The size of the initial particles increases slightly with the larger bromide concentration. Hollow particles are obtained in both cases. (E) Dependence of the diameter of the shown nickel and nickel phosphide nanoparticles and their inner cavity on the number of bromide ions relative to nickel atoms present during their synthesis. The error bars correspond to the standard deviations of the measured diameters. It can be seen that the overall particle size is slightly increased with larger amounts of the halide. There is no noticeable difference between the resulting particle sizes from syntheses with tetradodecylammonium chloride (TDAC) or tetradodecylammonium bromide (TDAB). Potentially, the nanoparticles formed in the presence of bromide ions tend to be slightly smaller. (F) X-ray diffraction patterns of the nanoparticle samples synthesised in the presence of different amounts of bromide ions. The resulting nickel (PDF card #: 01-087-0712) crystallite size increases with the amount of bromide. (G) X-ray diffraction patterns of the corresponding nanoparticle samples after crystallisation at 300 °C. The obtained nickel phosphide crystal phase is a mixture of $Ni_{12}P_5$ (PDF card #: 01-074-6017) and Ni_2P (PDF card #: 00-003-0953), while in case of larger halide amounts Ni_2P is found almost exclusively.

5. TEM and XRD Analysis of Samples Synthesised with Oleylamine of Different Purity

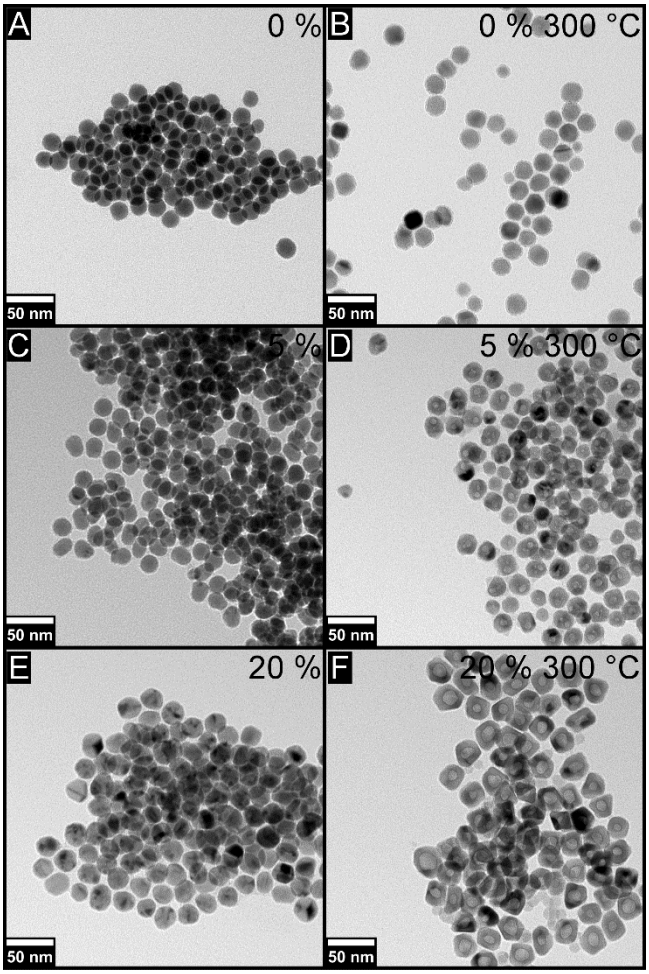

Fig. S7 TEM micrographs of Ni/Ni_xP_y particles synthesised using oleylamine of 70 % purity in the presence of different amounts of chloride ions. The usual trend of more crystalline nickel particles and hollower resulting nickel phosphide nanocrystals with increasing halide concentration can be observed.

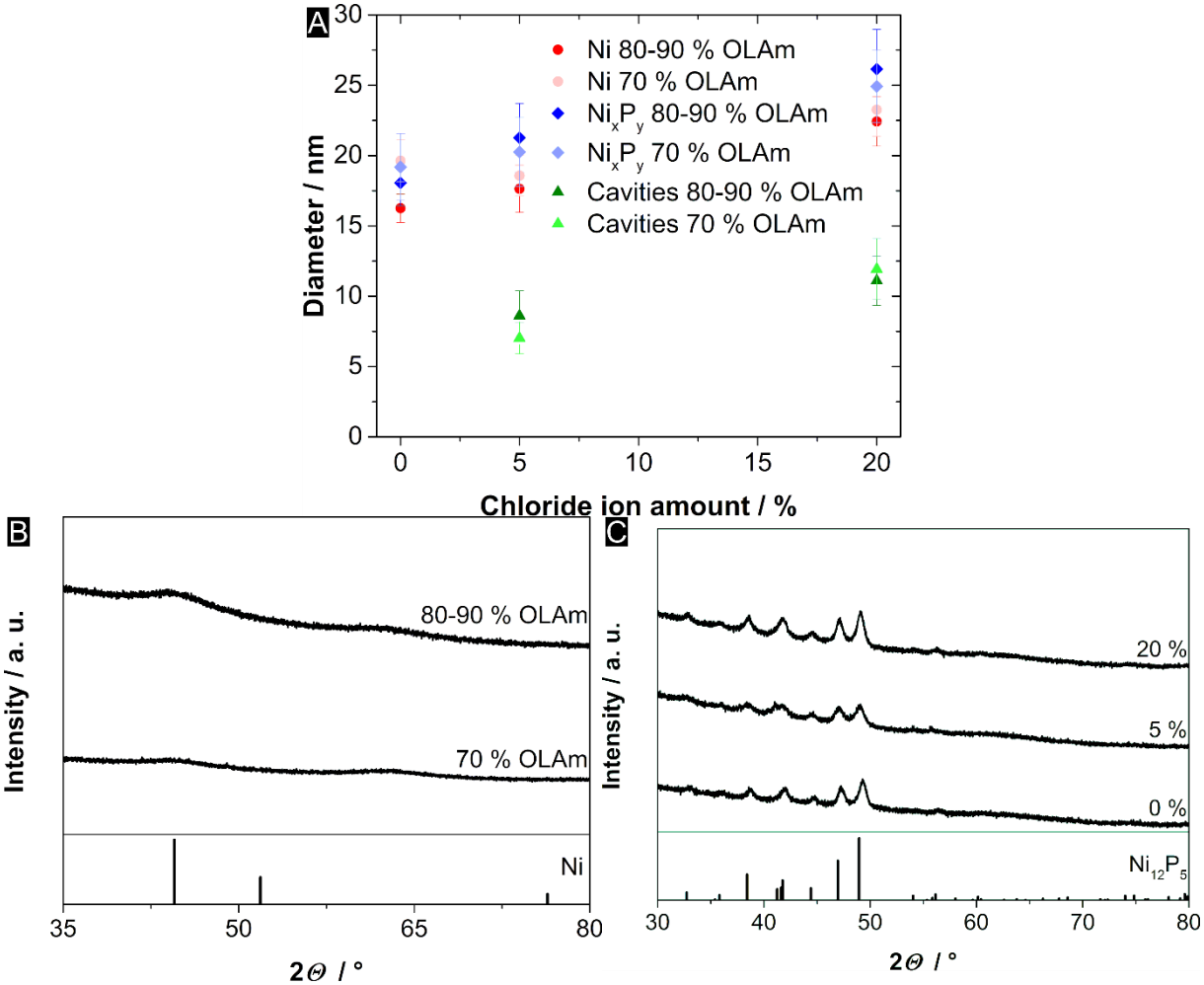

Fig. S8 (A) Dependence of the diameter of nickel nanoparticles, the corresponding nickel phosphide nanocrystals, and their inner cavity on the amount/purity of oleylamine (OLAm) present during their synthesis. The error bars correspond to the standard deviations of the measured diameters. It can be seen that in case of both OLAm purities the overall particle size is slightly increased with larger amounts of the halide. While the particles synthesised without any chloride are expectedly larger in case of the less pure OLAm, no large difference for the other samples can be seen. (B) X-ray diffraction patterns of the nanoparticle samples synthesised in the presence of oleylamine (OLAm) of different purity. The resulting nickel (PDF card #: 01-087-0712) crystallite size seems to be slightly larger in case of the purer OLAm. (C) X-ray diffraction patterns of the respective nanoparticle samples crystallised in the presence of less pure OLAm (70 %) and different amounts of TDAC. The obtained nickel phosphide crystal phase for all halide ion concentrations is $Ni_{12}P_5$ (PDF card #: 01-074-6017).

6. TEM and XRD Analysis of Samples Synthesised in Different Solvents

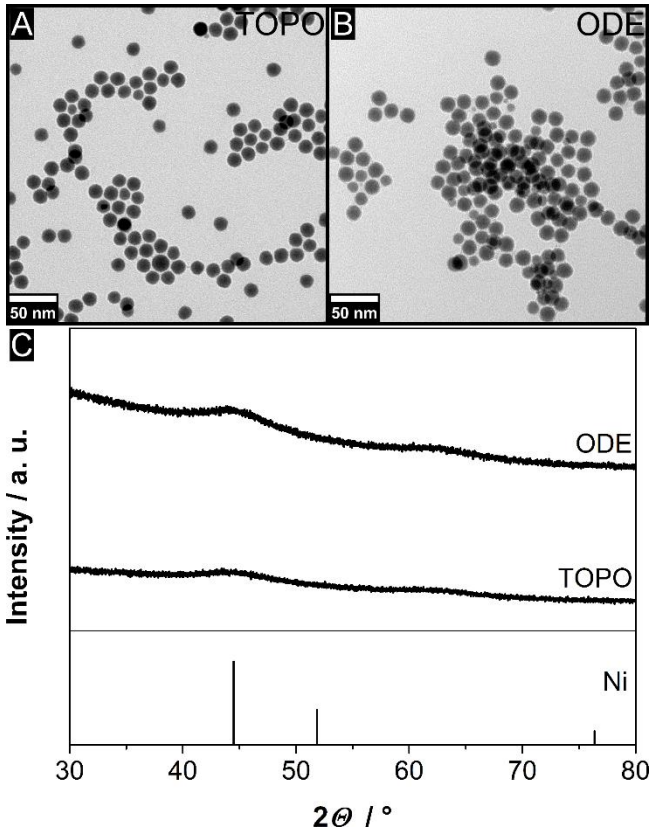

Fig. S9 TEM micrographs of Ni particles synthesised with TOPO (A, average particle diameter of 16.3 ± 1.0 nm) and ODE (B, average particle diameter of 15.2 ± 1.5 nm) used as the solvent for the synthesis. (C) X-ray diffraction patterns of the corresponding samples. Both nanoparticle batches are mostly amorphous but in case of the ODE, the very broad Ni (1 1 1) reflection (PDF card #: 01-087-0712) at around 45 °2ϑ is possibly slightly more pronounced. However, these results strongly suggest that the observed incorporation of phosphorus into the nanoparticles leading to their amorphous nature is mainly due to the presence of TOP and not caused by the usage of TOPO as the solvent for the reaction.

7. TEM Overview Images of Nickel Phosphide Nanoparticles

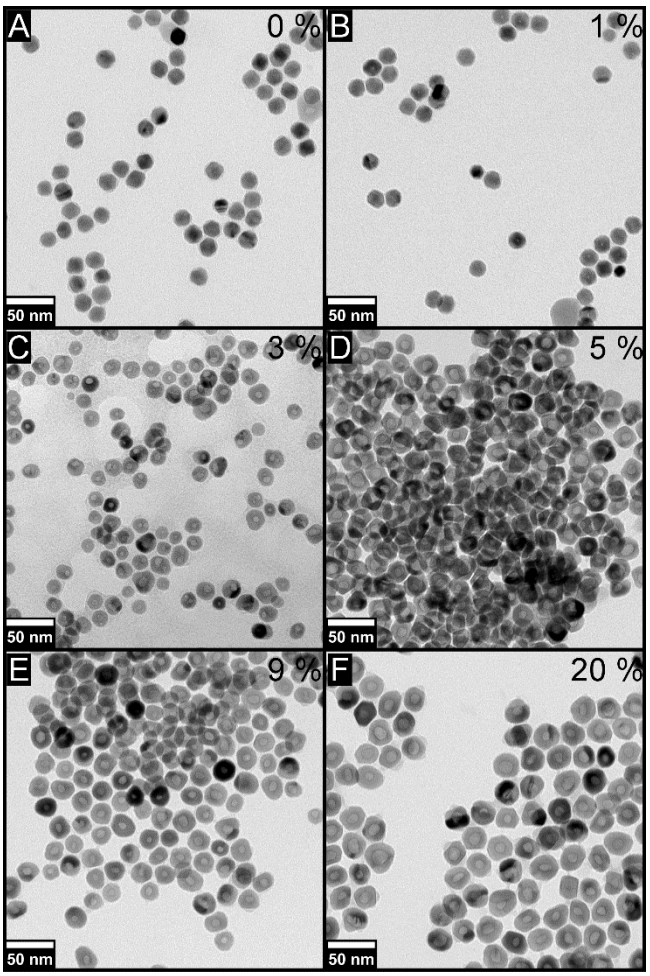

Fig. S10 TEM overview images of nickel phosphide nanoparticles crystallised in the presence of different concentrations of chloride ions (TDAC). With an increasing amount of chloride present the size of the particle cavities, formed via the nanoscale Kirkendall effect, is growing and hollow nanocrystals are obtained. Interestingly, in case of low chloride concentrations, the nanoparticles often have multiple cavities owing to small Ni crystallites in the precursor nanoparticles, which were probably located at a certain distance apart from each other.

8. Diameters of Particles Crystallised in the Presence of 1-dodecanethiol

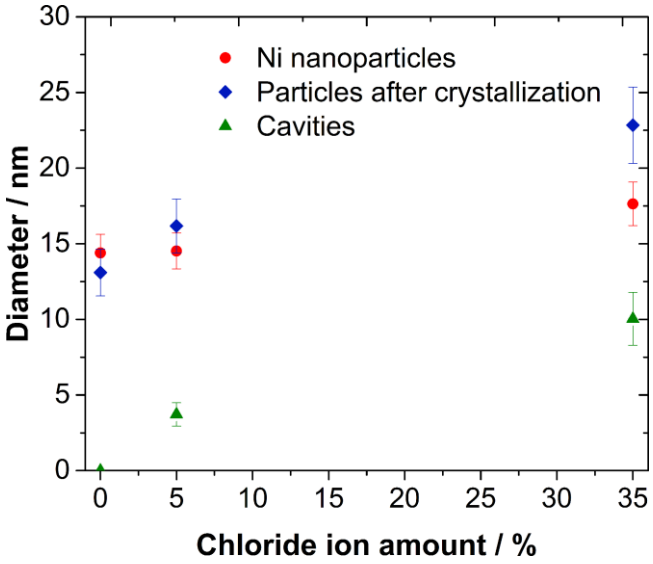

Fig. S11 Dependence of the diameter of nickel nanoparticles, the corresponding nickel phosphide or nickel sulphide nanocrystals, and their inner cavity on the number of chloride ions present during their synthesis after the addition of 1-dodecanethiol (DDT). The error bars correspond to the standard deviations of the measured average diameters. It can be seen that similar to the system without DDT the diameter of the cavities formed via the nanoscale Kirkendall effect is dependent on the chloride concentration. However, it should be noted that in the case of the sample with 5 % chloride multiple cavities often exist within a single particle and it is quite difficult to measure their actual size correctly.

9. Optical Spectroscopy of Nickel and Nickel Phosphide Nanoparticles

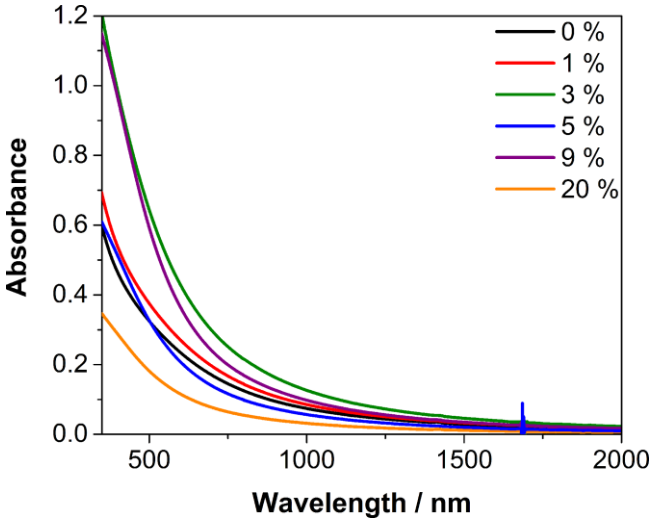

Fig. S12 UV/vis/NIR absorbance spectra of Ni particles in colloidal solution (toluene) synthesised in the presence of different amounts of chloride ions. In all cases, the absorbance rises towards shorter wavelengths due to the localised surface plasmon resonance of Ni which is located in the UV regime of the electromagnetic spectrum and outside of the possible measuring range for toluene.

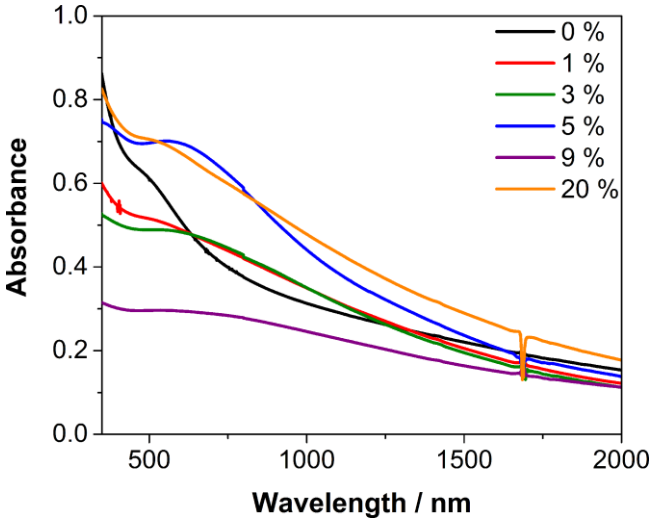

Fig. S13 UV/vis/NIR absorbance spectra of Ni_xP_y particles in colloidal solution (toluene) crystallised in the presence of different amounts of chloride ions. An absorbance shoulder can be seen at around 500 nm in case of the sample synthesised in the absence of halides while especially the nanoparticles produced with higher amounts of chloride in the synthesis show stronger absorbance at longer wavelengths. Due to the size of the particles, this cannot be explained exclusively by light scattering. However, since both $Ni_{12}P_5$ and Ni_2P show metallic behaviour at room temperature a possible explanation is the existence of a localised surface plasmon resonance with a very broad absorbance band like it is the case for small nickel sulphide nanoparticles.[4–8] Further experiments would be needed to confirm this theory.

10. Particles Crystallised in the Presence of Elemental S

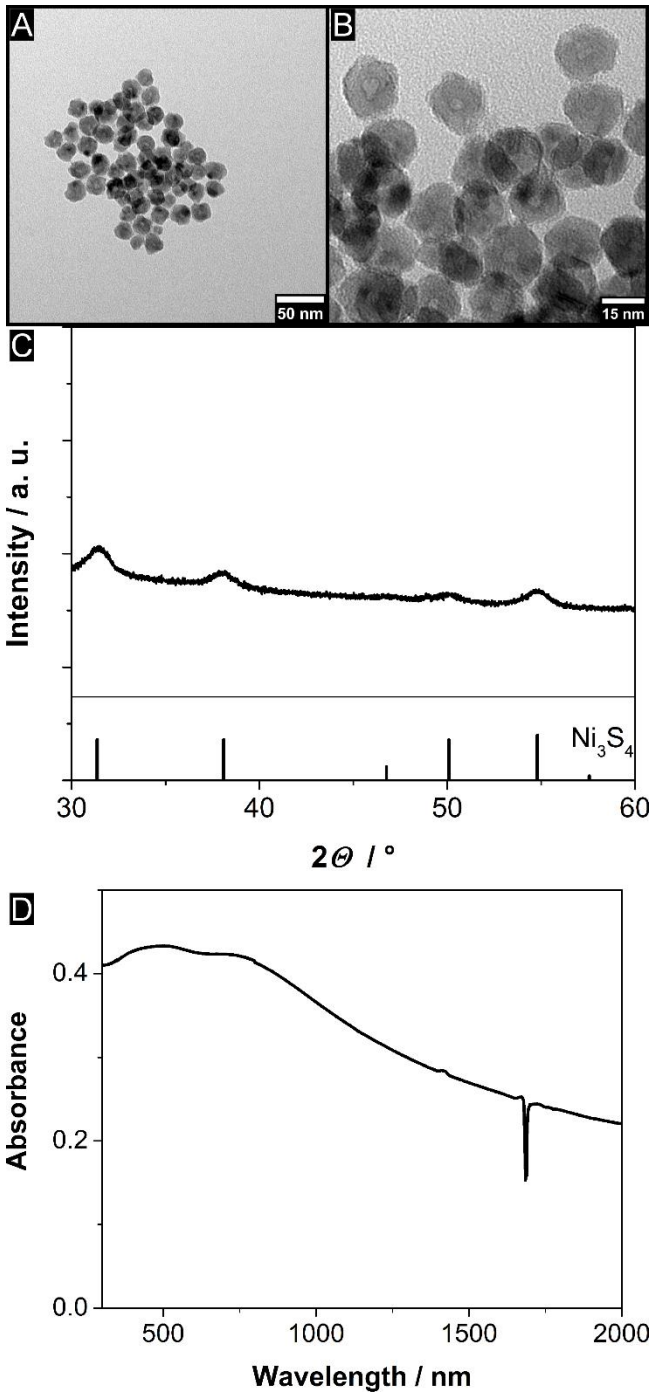

Fig. S14 TEM overview image (A) and HR-TEM micrograph (B) of nanoparticles crystallised in the presence of S and 40% chloride. Hollow and polycrystalline nanoparticles with a tendency to agglomerate are obtained. In the XRD pattern of the sample (C) it is visible that the formed phase is Ni_3S_4 (PDF card #: 00-008-0106). The UV/vis/NIR absorbance spectrum (D) of the particles shows a LSPR band at slightly below 500 nm which is typical for Ni_3S_4 and a shoulder at longer wavelengths which could be due to plasmonic coupling in nanoparticle aggregates. Additionally to aggregation, the broader linewidth of these particles compared to the Ni_3S_2 nanocrystals could be explained by the polycrystalline nature of the obtained Ni_3S_4 which leads to stronger damping processes. The only synthetic differences to the Ni_3S_2 procedure are a change of the solvent from TOPO to ODE and the substitution of DDT by 5 mL of a mixture of S dispersed in ODE (0.2 M).

11. HR-TEM Comparison of Hollow Ni_3S_2 and Ni_3S_4 Nanoparticles

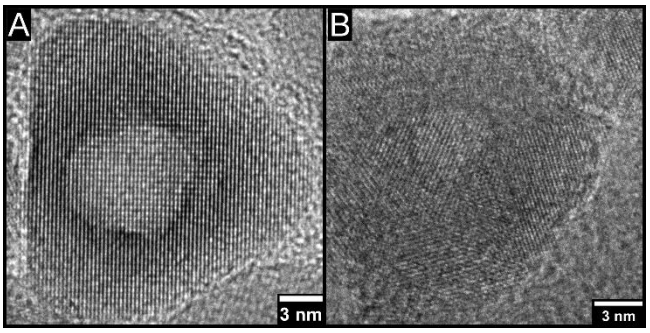

Fig. S15 HR-TEM images of representative hollow Ni_3S_2 (A) and Ni_3S_4 (B) nanoparticles crystallised in the presence of 40% chloride. It can be seen that while the Ni_3S_2 particle is single-crystalline the Ni_3S_4 pendant consists of multiple smaller crystallites.

References

1 T. Iwamoto, A. Nagao, K. Kitagishi, S. Honjo and B. Jeyadevan, *J. Phys. Chem. Solids*, 2015, **87**, 136–146.

2 H. Winnischofer, T. C. R. Rocha, W. C. Nunes, L. M. Socolovsky, M. Knobel and D. Zanchet, *ACS Nano*, 2008, **2**, 1313–1319.

3 J.-J. Li, M.-C. Liu, L.-B. Kong, D. Wang, Y.-M. Hu, W. Han and L. Kang, *RSC Adv.*, 2015, **5**, 41721–41728.

4 I. Shirotani, E. Takahashi, N. Mukai, K. Nozawa, M. Kinoshita, T. Yagi, K. Suzuki, T. Enoki and S. Hino, *Jpn. J. Appl. Phys.*, 1993, **32**, 294.

5 S. Ishida, Y. Sugizaki, T. Nakamura, K. Edamoto, M. Matsunami, T. Hajiri and S. Kimura, *e-Journal Surf. Sci. Nanotechnol.*, 2015, **13**, 93–98.

6 J. S. Chen, C. Yu, H. Lu and J. M. Chen, *Phase Transitions*, 2016, **89**, 1078–1089.

7 Q. Yuan, H. Ariga and K. Asakura, *Top. Catal.*, 2015, **58**, 194–200.

8 R. Himstedt, P. Rusch, D. Hinrichs, T. Kodanek, J. Lauth, S. Kinge, L. D. A. Siebbeles and D. Dorfs, *Chem. Mater.*, 2017, **29**, 7371–7377.